TOXICOLOGICAL SCIENCES, 164(1), 2018, 101–114

doi: 10.1093/toxsci/kfy064
Advance Access Publication Date: April 5, 2018
Research Article

Respirable Uranyl-Vanadate-Containing Particulate Matter Derived From a Legacy Uranium Mine Site Exhibits Potentiated Cardiopulmonary Toxicity

Katherine E. Zychowski,* Vamsi Kodali,† Molly Harmon,* Christina R. Tyler,‡ Bethany Sanchez,* Yoselin Ordonez Suarez,* Guy Herbert,* Abigail Wheeler,* Sumant Avasarala,§ José M. Cerrato,§ Nitesh K. Kunda,* Pavan Muttil,* Chris Shuey,¶ Adrian Brearley,‖ Abdul-Mehdi Ali,‖ Yan Lin,‖| Mohammad Shoeb,† Aaron Erdely,† and Matthew J. Campen*,[1]

*Department of Pharmaceutical Sciences, University of New Mexico-Health Sciences Center, Albuquerque, New Mexico 87131; †Health Effects Laboratory Division, National Institute for Occupational Safety and Health, Morgantown, West Virginia; ‡Biosciences Division, Los Alamos National Laboratories, Los Alamos, New Mexico 87545; §Department of Civil Engineering, University of New Mexico, Albuquerque, New Mexico 87131; ¶Southwest Research and Information Center, Albuquerque, New Mexico 87196; and ‖Department of Earth and Planetary Sciences and ‖|Department of Geography, University of New Mexico, Albuquerque, New Mexico 87131

[1]To whom correspondence should be addressed at Department of Pharmaceutical Sciences, College of Pharmacy, MSC09 5360, 1 University of New Mexico, Albuquerque, NM 87131-5691. Fax: 505-272-6749; E-mail: mcampen@salud.unm.edu.

ABSTRACT

Exposure to windblown particulate matter (PM) arising from legacy uranium (U) mine sites in the Navajo Nation may pose a human health hazard due to their potentially high metal content, including U and vanadium (V). To assess the toxic impact of PM derived from Claim 28 (a priority U mine) compared with background PM, and consider the putative role of metal species U and V. Two representative sediment samples from Navajo Nation sites (Background PM and Claim 28 PM) were obtained, characterized in terms of chemistry and morphology, and fractioned to the respirable ($\leq$ 10 μm) fraction. Mice were dosed with either PM sample, uranyl acetate, or vanadyl sulfate via aspiration (100 μg), with assessments of pulmonary and vascular toxicity 24 h later. Particulate matter samples were also examined for *in vitro* effects on cytotoxicity, oxidative stress, phagocytosis, and inflammasome induction. Claim 28 PM_{10} was highly enriched with U and V and exhibited a unique nanoparticle ultrastructure compared with background PM_{10}. Claim 28 PM_{10} exhibited enhanced pulmonary and vascular toxicity relative to background PM_{10}. Both U and V exhibited complementary pulmonary inflammatory potential, with U driving a classical inflammatory cytokine profile (elevated interleukin [IL]-1β, tumor necrosis factor-α, and keratinocyte chemoattractant/human growth-regulated oncogene) while V preferentially induced a different cytokine pattern (elevated IL-5, IL-6, and IL-10). Claim 28 PM_{10} was more potent than background PM_{10} in terms of *in vitro* cytotoxicity, impairment of phagocytosis, and oxidative stress responses. Resuspended PM_{10} derived from U mine waste exhibit greater cardiopulmonary toxicity than background dusts. Rigorous exposure assessment is needed to gauge the regional health risks imparted by these unremediated sites.

Key words: uranium; vanadium; cytokines; immunotoxicology; inflammation; immunotoxicology; particulates; respiratory toxicology; cardiopulmonary; respiratory toxicology.

Since the Cold War era, the Navajo Nation is home to over 500 abandoned uranium (U) mines, which remain potential sources of heavy metal contamination due to inconsistent or incomplete remediation (Dawson *et al.*, 1997; DeLemos *et al.*, 2009). Although U-containing minerals such as uraninite and carnotite are naturally occurring in this region (Stokes, 1951), mining operations that extracted these ores without proper reclamation have left areas of concern adjacent to Navajo residences. Consequently, the Navajo population has been subject to varying degrees of U, vanadium (V), and arsenic (As) exposure (Brugge *et al.*, 2007; Hoover *et al.*, 2017; Lewis *et al.*, 2017). These metals have been shown to cause toxicity to kidneys, the nervous system, and cardiovascular tissues (Campen *et al.*, 2001; Homma-Takeda *et al.*, 2015; Nadadur *et al.*, 2009; Ngwa *et al.*, 2014; Poisson *et al.*, 2014; Saint-Marc *et al.*, 2016; Vicente-Vicente *et al.*, 2010); however, the ultimate impact of chronic, low-level, mixed metals exposure on affected communities is unclear.

We recently observed that residential proximity to abandoned U mine sites was significantly associated with cumulative circulating inflammatory potential in the serum of local residents (Harmon *et al.*, 2017). Although chronic exposure to mining-based metal mixtures could occur through multiple routes, including ingestion via food or drinking water, these findings linking inflammation and residential proximity suggested inhalation of resuspended particulate matter (PM) may be an underappreciated environmental risk for local communities (Harmon *et al.*, 2017). Aeolian transport and dust storms in the Southwestern United States have been increasing in recent years due to climate change, and this environmental trend is projected to continue into the foreseeable future (Munson *et al.*, 2011; Stovern *et al.*, 2014). Health effects from U mining in this region have largely focused on cancers, in particular radiation-related lung cancer in miners subsequent to chronic occupational exposure (Brugge *et al.*, 2005; Mulloy *et al.*, 2001). Other disorders that have been heavily studied following U exposure include renal, developmental, reproductive, diminished bone growth, and DNA damage (Arfsten *et al.*, 2001; Brugge *et al.*, 2005).

However, in recent decades, there has been a notable increase in cardiovascular and metabolic disease in the Navajo population, with only limited inquiry into possible contributions from environmental contaminants (Gittelsohn *et al.*, 2013; Harmon *et al.*, 2016; Percy *et al.*, 1997). Although many lifestyle and genetic factors contribute to cardiovascular disease, there is also a strong link between airborne PM exposure and both acute and chronic cardiovascular disease (Brook *et al.*, 2010; Peters and Pope, 2002; Pope *et al.*, 2003), and metallic components of PM are clear modifiers of toxicity (Bell *et al.*, 2009; Dominici *et al.*, 2007; Lippmann *et al.*, 2006). In the desert Southwestern United States, metal-bearing PM from mine sites are of a markedly different chemical/mineralogical character than metal-bearing PM from more urbanized regions, especially near industrial sea port regions. Such mineralogical and chemical differences in PM-associated metals are relatively unstudied from a toxicological perspective.

Blake *et al.* (2015) recently reported elevated concentrations of U and V in water and solid from the Claim 28 U mine site in the Blue Gap Tachee chapter of Navajo Nation, showing substantial mobility of U and V in the region. This study also identified U-V-bearing solids in these mine wastes that are similar to the mineral carnotite [$K_2(UO_2)_2(VO_4)_2{\cdot}3H_2O$]. Using samples derived from this region, we characterized the physicochemistry of respirable PM from sediments in this region and tested the respiratory and vascular toxicity thereof, as compared with a background PM not impacted by the mine site contamination. We hypothesized that residual U ore contaminants in the mine site soils would exhibit a potentiated toxicity relative to respirable PM derived from naturally occurring background sediments.

MATERIALS AND METHODS

PM_{10} Derivation From Regional Sediments

Sediment samples were procured from 2 locations: Claim 28 mine site and from the canyon floor approximately 2 km away in the Blue Gap Tachee Chapter of Navajo Nation (Figure 1). Claim 28 and its proximal watershed region have been recently characterized in terms of the occurrence and mobility of mining-related metals. Sediment samples were collected from the top 30 cm from the ground level of the Claim 28 mine site, as described previously (Blake *et al.*, 2015). The background reference sample was collected from an area that is not impacted by historical mining activities or drainage from the mine site but may be influenced by windblown contaminants.

A next-generation impactor (NGI, model 170 NGI, MSP Corporation, Shoreview, Minnesota) fitted with preseparator and gravimetric cups was employed to collect fraction of grains from the mine waste and background sediment samples small enough to deposit in the respirable airways (ie, PM smaller than 4.46 μm mass mean aerodynamic diameter). Briefly, the mine waste and background samples were weighed and manually loaded into the hydroxypropyl methylcellulose capsules (VCaps, size 3, Capsugel, USA). A total of 10 capsules, each containing 100 mg of powder, were filled. Each capsule was placed in an Aerolizer and the sample was drawn through the induction port using a pump (Copley Scientific, Nottingham, UK) operated at a flow rate of 60 l/min for 4 s. Following aerosolization, powder deposition on each stage was determined gravimetrically. The powders deposited from stages 3 to 8 correspond to an aerodynamic particle size $d_{ae} < 4.46$ μm. These powders were reconstituted in dispersion media (DM) as the aqueous vehicle (0.6 mg/ml mouse serum albumin and 10 μg/ml 1, 2-dipalmitoyl-sn-glycero-3-phosphocholine in phosphate-buffered saline), with sonication for 5 min to ensure dispersion and used for pharyngeal aspiration in mice.

Chemical and Morphological Characterization of Mine Site-Derived PM_{10}

Acid digestions were performed to measure the total acid extractable trace metal concentrations within the PM_{10} fraction of both mine waste and background samples. The acid digestion protocol involved addition of 3 ml of hydrochloric acid, 2 ml of nitric acid, and 2 ml of hydrofluoric acid into 50 ml digestion tubes containing up to 2 ml dispersions of respirable sediment fractions (< 10 μm) in DM at a 2 mg/ml concentration. The digestion tubes were then heated using a Digi prep MS SCP Science block digester at 95°C for 2 h, followed by dilution of acid extracts to 50 ml. The samples were then filtered using 0.45 μm

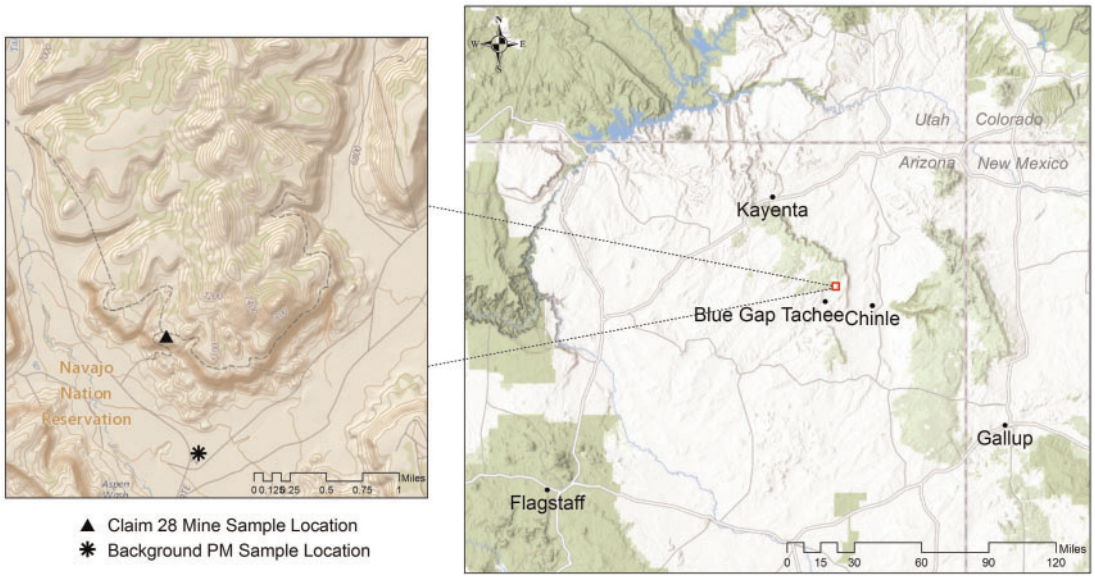

Figure 1. Location of Claim 28 mine site in the Blue Gap Tachee Chapter of the Navajo Nation. Triangle (▲) and asterisks (*) in inset map denote location of sediment sampling for mine site and background particulate matter (PM). (Data Sources: Esri, HERE, DeLorme, increment P Corp., NPS, NRCan, Ordnance Survey, OpenStreetMap contributors, USGS, NGA, NASA, CGIAR, N Robinson, NCEAS, NLS, OS, NMA, Geodatastyrelsen, Rijkswaterstaat, GSA, Geoland, FEMA, Intermap and the GIS user community; USGS The National Map: National Boundaries Dataset, 3DEP Elevation Program, Geographic Names Information System, National Hydrography Dataset, National Land Cover Database, National Structures Dataset, and National Transportation Dataset; U.S. Census Bureau—TIGER/Line; and USFS Road Data).

filters to remove any suspended or undissolved solids and diluted accordingly for assessing the trace metal concentrations.

The assessment included measuring bulk and trace concentrations of U and its cooccurring metals (U, As, Cr, Cu, V, Ni, Pb, Cd, Al, Si, and Ca) using inductively coupled plasma—optical emission spectroscopy (ICP-OES; PerkinElmer Optima 5300DV) and mass spectroscopy (ICP-MS; PerkinElmer NexION 300D, Dynamic Reaction Cell). Both ICPs are calibrated with a 5-point calibration curve and QA/QC measures are taken to ensure quality results. To avoid spectral interference, arsenic oxide (AsO) was assessed at *m/z* 91.

High-resolution transmission electron microscopic (HR-TEM) analysis was conducted on the mine waste sample to observe the presence and crystallinity of U-V nanomineral phases in the respirable fraction of the Blue Gap/Tachee mine waste sediments using its energy dispersive spectroscopy (EDS) and selected area electron diffraction (SAED) capabilities. Transmission electron microscopic analysis was performed using a JEOL 2010 HR-TEM fitted with a GATAN Orius high-speed CCD camera and an Oxford INCA system with an ultra-thin window EDS detector. PM_{10} were allowed to deposit onto standard holey carbon film-covered copper TEM grids adhered to the collection plates of the NGI. These Cu grids were then fixed onto a regular TEM holder and loaded into the HR-TEM where the EDS detector was used to identify the U-V mineral phases by obtaining the elemental composition of a specific grain and SAED technique was used to provide information on its crystallinity.

In Vitro *Assessments of Toxicity*

Cell culture. Human peripheral blood monocyte cell line, THP-1 cells, were cultured, differentiated, and primed using procedures described previously (Xia *et al.*, 2013). In brief, human monocyte THP-1 cells (ATCC No. TIB 202) were grown in RPMI-1640 media supplemented with 10% fetal bovine serum (FBS), 100 μg/ml Penicillin-Streptomycin, and 50 μM of beta-mercaptoethanol. NLRP3-deficient (defNLRP3) THP-1 cells were purchased from InvivoGen (San Diego, California) and grown in RPMI-1640 media supplemented with 10% FBS and 100 μg/ml Penicillin-Streptomycin, and 300 μg/ml hygromycin. THP-1 cells were differentiated into macrophages by treating them with vitamin D3 at 150 nM overnight and then 5 nM PMA for 12 h. As described (Xia *et al.*, 2013) differentiated THP-1 cells were primed by coexposing PM with 10 ng/ml LPS to induce the transcription of pro-IL-1β.

Cytotoxicity, oxidative stress, caspase-1, high content, and electron microscopy. Membrane integrity of the cells after PM exposure was assessed using CytoTox-One homogenous membrane integrity assay (Promega, Madison, Wisconsin).

Active caspase-1 was quantified using a fluorochrome inhibitor of caspase-1 (FAM-YVAD-FMK) according to manufacturer's recommendations (Immunochemistry Technologies LLC, Bloomington, Minnesota). Ten thousand THP-1 cells were plated and differentiated to macrophages on a glass bottom 96-well plate (Greiner Bio-One, Monroe, North Carolina). Cells were then challenged with PM_{10} (0–200 μg/ml) for 6 h, washed twice with PBS, and incubated with fresh media containing a cocktail containing Hoechst 33342 (1 μM) and FAM-YVAD-FMK for 30 min at 37°C. After incubation the 96-well plate was washed 3 times and imaged using a high content screening epifluorescence microscope Image-Xpress micro (Molecular Devices, Sunnyvale, California). Images were collected using DAPI and FITC filter/dichroic combinations to image Hoechst 33342 (blue) and FAM-YVAD-FMK (green), respectively, under ×20 magnification. The microscopic images were automatically analyzed by MetaXpress software. The caspase-1 positive percent or the intensity of caspase-1 was calculated based on the total cell number (Hoechst 33342 positive cells).

Reactive oxygen species (ROS) generated during particle exposure was evaluated using dihydroethidium (DHE, Molecular Probes, Eugene, Oregon). After challenging the cells with the PM_{10} (0–200 μg/ml) for 4 h, cells were fixed in formalin (10% in PBS, Fisher Scientific, Fair Lawn, New Jersey), rinsed with PBS, and incubated with 2.5 μmol/l DHE for 15 min. Cells were

washed in PBS twice and mounted using ProLong Gold (Molecular Probes, Eugene, Oregon). As a secondary confirmation of the oxidative stress induced by particulate exposure, lipid peroxidation due to ROS, was evaluated using 4-hydroxynonenal (4-HNE). Cells were challenged with PM_{10} (0–200 μg/ml) for 24 h and fixed using 10% formalin for 15 min followed by a 5 min incubation with 10% formalin containing 0.3% Triton X-100. Cells were then rinsed in PBS and nonspecific adsorption was blocked by 2% BSA. 4-HNE was then tagged using anti–4-HNE antibody (ab46545, Abcam, Cambridge, UK) for 12 h, washed with PBS and fluorescently tagged using secondary antibody (Ab150077, Abcam, Cambridge, UK) for 45 min. Finally, cells were washed in PBS twice and mounted using ProLong Gold (Molecular Probes, Eugene, Oregon). Images were taken using an Olympus AX70 upright microscope, and quantification was performed using cellSens Dimension1.15 software (Olympus Corporation, Tokyo, Japan).

For obtaining electron microscopy images of THP-1 cells with PM_{10}, THP-1 macrophages were exposed to PM_{10} at 100 μg/ml for 24 h. The cells were then washed twice with PBS and fixed with Karnovsky's fixative buffered in 0.1 M sodium cacodylate. Cells were then postfixed in 1% osmium tetroxide, stained en bloc with 1% tannic acid and 0.5% filtered uranyl acetate, dehydrated with a graded series of ethanol, infiltrated with propylene oxide and LX-112 epon resin, and finally embedded in LX-112 epon. Sections were cut at 70 nm, placed on 200 mesh copper grids, and stained with 4% uranyl acetate and Reynolds' lead citrate. Images were taken using a JEOL JEM 1400 TEM (JEOL USA) with an AMT XR-81M-B digital camera attachment.

IL-1β cytokine analysis. Interleukin (IL)-1β production in differentiated and primed THP-1 culture supernatants exposed to PM_{10} (0–200 μg/ml) for 24 h was determined using Human IL-1 beta/IL-1F2 Quantikine ELISA (Cat No. DLB50, R&D Systems, Minneapolis, Minnesota) following the manufacturers recommendation.

Phagocytosis functional assay. Modification in phagocytic capacity of macrophages exposed to PM_{10} was evaluated by challenging PM_{10}-exposed macrophages with *Escherichia coli* GFP (ATCC No. 25922GFP). The differentiated and primed THP-1 cells were exposed to various concentrations of PM_{10} (0–200 μg/ml) for 24 h and were further challenged with fresh medium containing *E. coli* GFP at multiplicity of infection of 1:25. In order for the bacteria to reach the cells at the bottom of the well, the plate containing the cells and bacteria was centrifuged at 1000 × g for 10 min before placing them in an incubator at 37°C. After 2 h of challenge, the cells were washed with PBS, harvested by trypsinization and scraping, centrifuged at 1000 × g for 5 min, and resuspended in PBS. The cell-associated bacteria were quantified using a BD LSR II flow cytometer (BD Biosciences, San Diego, California). All experiments were performed using triplicate samples and at least 10 000 cells were analyzed per treatment. The mean fluorescence was determined using FlowJo (FlowJo LLC, Ashland, Oregon).

Aspiration Exposure

Male, 6- to 8-week-old C57BL/6 mice were purchased from Taconic Laboratories. Mice were held on a 12:12 h light:dark cycle in an AAALAC-approved facility with food and water available *ad libitum*. All studies were conducted with approval from the University of New Mexico Institutional Animal Care and Use Committee.

Immediately prior to oropharyngeal aspiration, particulate size in the DM vehicle was characterized and confirmed to be < 10 μm by dispersive light scattering. C57BL/6 mice were exposed to 100 μg of PM_{10} sample in 50 μl of vehicle using oropharyngeal aspiration, a technique that allows deep and even distribution of particulates into the lungs. Briefly, mice were anesthetized with low-dose isofluorane, removed from anesthesia, and suspended at an approximately 45° angle. The PM sample was then pipetted into the back of the throat with tongue extended to prevent swallowing and with nasal passages briefly manually occluded until the droplet of sample was fully aspirated, just as mice were awaking from anesthesia. Three exposure groups consisted of DM (control), Claim 28 PM_{10}, or Background PM_{10} (100 μg/mouse).

In a secondary study, mice were aspirated with 0.22 μmol U or V in the form of dissolved uranyl acetate and vanadyl sulfate (VOSO4; Sigma-Aldrich, Saint Louis, Missouri). This concentration was chosen as analogous to the amount of U and V predicted in 100 μg of pure carnotite mineral, as a worst-case scenario. For both studies, mice were euthanized 24 h postaspiration and tissues were collected for remaining experiments.

Pulmonary Outcomes

A cannula was inserted through the trachea and phosphate-buffered saline was injected and withdrawn using a 1 ml sterile syringe to collect bronchoalveolar lavage fluid (BALF) and cells. Total cell counts and neutrophil counts were immediately obtained from 6 to 8 subjects per group. Bronchoalveolar lavage fluid samples from lungs that leaked excessively during the procedure were not included in the final analysis. Total protein was analyzed in the BALF using Bradford's assay (Bradford, 1976). All assays were performed in triplicate, as previously described (Robertson *et al.*, 2013). Cytokines interferon-γ (IFN-γ), IL-10, IL-12p70, IL-1β, IL-2, IL-4, IL-5, IL-6, keratinocyte chemoattractant/human growth-regulated oncogene (KC/GRO), and tumor necrosis factor-alpha (TNF-α) were measured in BALF and serum from 6 subjects per group using an electrochemiluminescence multiplex platform, according to manufacturer's instructions (Meso Scale Diagnostics, Rockville, Maryland).

Ex Vivo *Vasoreactivity*

Twenty-four hours postoropharyngeal aspiration, aortic rings were cleaned and dissected from mice to assess serotonin-mediated vasoconstriction, as previously described (Aragon *et al.*, 2016; Paffett *et al.*, 2015). Ring segments (2–3 mm) were mounted on a myograph (610 M; DMT Inc, Atlanta, Georgia), submerged in physiological saline solution (PSS; 119 mM NaCl, 25 mM $NaHCO_3$, 5.5 mM glucose, 4.7 mM KCl, 1.2 $MgSO_4$, 1.2 mM $KHPO_4$, 0.027 mM EDTA, 2.5 mM $CaCl_2$) bubbled with carbogen (21%O_2–6%CO_2-balance N_2) at 37°C. These aortic rings were then equilibrated in carbogen-bubbled PSS for 30 min at 2 g of tension. Afterwards, vessel normalization commenced by gradually increasing tension in 2 mN intervals over 5 min to eventually achieve a passive tension of 10 mN. Vessels then equilibrated in fresh PSS for 30 min. High potassium PSS (KPSS 64.9 mN NaCl, 25.0 mN $NaHCO_3$, 5.5 mN glucose, 58.9 mN KCl, 1.2 mN $MgSO_4$, 1.2 mN KH_2PO_4, 0.027 mN EDTA, 2.5 mN $CaCl_2$) was applied to contract vessels and confirm viability. After an additional 30 min equilibration, vessels were gradually contracted with increasing concentrations of serotonin (10^{-9}–10^{-5} M) over the course of 5 min intervals.

To test the endothelial effects of circulating compounds arising postexposure, naïve mice were anesthetized and aortic rings were dissected as described earlier. Following equilibration,

vessels were constricted with 1% serum from mice exposed to either vehicle, Claim 28 PM_{10}, or Background PM_{10}. Acetylcholine (ACh) was then incrementally added in half-log concentration increases (10^{-9}–10^{-5} M) at 5 min intervals. Data were acquired using a MacLab/4e analog-digital convertor displayed through LabChart software (AD Instruments, USA). Both contraction and relaxation data are expressed as a percentage of serum-induced contraction, with subtracted baseline tension.

In a second set of experiments, thoracic aortas were dissected from mice previously exposed to uranyl acetate (0.22 μmol) and vanadate sulfate (0.22 μmol). Using the aforementioned vasoreactivity assay, aortic rings were mounted and subject to U46619 (Cayman Chemical, Ann Arbor, Michigan) constriction for approximately 20 min and ACh vasorelaxation (10^{-9}–10^{-5} M) over the course of 5 min intervals. Relaxation data were then expressed as a percentage of U46619 contraction, with subtracted baseline tension.

Lung and Heart Transcriptional Responses to PM_{10}

Lungs and hearts from PM-aspirated mice were isolated, snap-frozen in liquid nitrogen and stored at −80°C and quantitative polymerase chain reaction (qPCR) methods were used to assess transcriptional changes (Aragon *et al.*, 2015). Briefly, lung and heart samples were homogenized and isolation of RNA was performed using a QIAGEN RNA minikit (QIAGEN, Valencia, California). High-capacity cDNA reverse transcriptase was used to reverse transcribed RNA, immediately prior to qPCR. The target probes (serum amyloid A-3 [Saa-3], IL-1β, IL-6, and TNF-α) were amplified using TaqMan Universal Master Mix. TATA box-binding protein (TBP) was utilized as the housekeeping gene. The $2^{-\Delta\Delta CT}$ method (Livak and Schmittgen, 2001) was used to analyze relative gene expression and the relative amount of mRNA for each sample was normalized to TBP.

Statistics

Most assays were compared via ANOVA with Tukey's multiple comparison test to consider differences between groups. *In vitro* studies utilized 2-factor ANOVAs, considering dose and particulate sample as the 2 factors, with Bonferroni *post hoc* testing to compare between Claim 28 and Background PM_{10}. For vascular relaxation and contraction assays, a repeated measures 2-factor ANOVA, considering exposure and agonist (ACh or 5-HT) as those 2 factors, was used with Tukey's *post hoc* multiple comparison test. P values $< .05$ were considered significant. Data presented in graphs are mean ± SEM.

RESULTS

Characterization of Mine Waste and Background Sediment and PM_{10}

Sample mineralogy was assessed by HR-TEM for both the mine waste and background sediments and the resuspended, isolated respirable PM_{10} fractions. No measureable radiation (ie, above background) could be detected in either PM_{10} sample. High-resolution transmission electron microscopic and EDS analysis indicated that mineralogical crystals from Claim 28 mine waste contained high levels of U and V (Figure 2). This was present in both the original sediment samples (Figs. 2A and 2B) as well as the fractionated respirable (approximately 100 nm) particle sizes (Figs. 2C and 2D). Further morphological characterization of the carnotite grains in the PM_{10} fraction from Claim 28 revealed an unexpected nanoparticulate ultrastructure (Figs. 2E, 2F, and 2G). LPS was assessed.

Using several mine site samples sieved to a < 63 μm diameter, we determined that metallic grains tended to associate with the smaller size fraction, as for all samples there was a relative enrichment of numerous trace elements in the small grains relative to the complete sample (Figure 3A). Dispersive light scattering size distribution analysis confirmed that the majority of particles collected by the NGI and suspended in DM were < 10 μm with an average of size between 1.5 and 4 μm (Figure 3B). Following confirmation of a respirable PM_{10} size range, ICP-MS analysis confirmed that the respirable PM fraction from the Claim 28 mine site contained much higher levels of U (approximately 8-fold greater) and V (approximately 50-fold greater) than PM from background samples (Figure 3C). Zeta potential was also assessed in PBS and media for Claim 28 mine waste PM_{10} (−9.9 ± 0.5 mV and −8.3 ± 0.5 mV, respectively) and background PM_{10} (−6.9 ± 1.3 mV and −6.4 ± 1.3 mV, respectively). These samples were then used for aspiration toxicology studies.

In Vitro Cytotoxicity of Claim 28 Mine Waste-Derived PM_{10}

Claim 28 mine waste-derived PM_{10} exhibited consistently greater toxicity to treated THP-1 cells compared with the Background PM_{10} (Figure 4). This was especially apparent for cellular LDH release (Figure 4A), which was significantly elevated at even the lowest concentrations of Claim 28 PM_{10} (1.5 μg/ml) and a sustained difference from background PM_{10} was evident out to high concentrations (200 μg/ml). We tested the extent to which this effect was driven by inflammasome activity using NLRP3-deficient THP-1 cells. LDH release induced by Claim 28 PM_{10} was partially dependent on NLRP3 mechanisms, suggesting that a more potent inflammasomal response may explain the differences between Claim 28 PM_{10} and background PM_{10}. Interestingly, the inflammasome contribution appeared most consequential at the highest doses, suggesting that at low doses other mechanisms are driving the LDH release.

General oxidative stress, as measured by DHE staining in THP-1 cells, was dramatically enhanced in Claim 28 PM_{10}-treated THP-1 cells compared with background PM_{10} (Figure 4B). Caspase 1 induction, both in terms of the percentage of cells expressing caspase 1 and the overall intensity of staining (Figure 4C), was elevated in Claim 28 PM_{10}-treated THP-1 cells compared with background PM_{10}. Claim 28 PM_{10} induced a mild increase in IL-1β release compared with background PM_{10}, and this was abolished in NLRP3-deficient THP-1 cells (Figure 4D). Furthermore, Claim 28 PM_{10} had a negative impact on phagocytic activity at low concentrations, while background PM_{10} had no net effect (Figure 4D). Lastly, Claim 28 PM_{10} treatment produced greater lipid peroxidation, as indicated by 4-HNE staining, compared with background PM_{10} (Figure 4E).

Pulmonary Effects Following Claim 28 Mine Waste PM_{10} Oropharyngeal Aspiration

Bronchoalveolar lavage cellularity. Mice were treated with 100 μg of the Claim 28 PM_{10} or background PM_{10}, and compared with DM controls at 24 h postexposure. Bronchoalveolar lavage fluid results indicate that neutrophil count and total cell count significantly increased in Claim 28 PM_{10}-treated mice when compared with vehicle control and background PM_{10}, and background PM_{10} induced a modest inflammatory response compared with control mice (Figs. 5A and 5B). Total macrophage numbers were unchanged between groups (data not shown, but reflected by the difference between total cells and neutrophil counts).

Bronchoalveolar lavage total protein and cytokines. Total protein content of lavage fluid, an indication of lung injury, was not

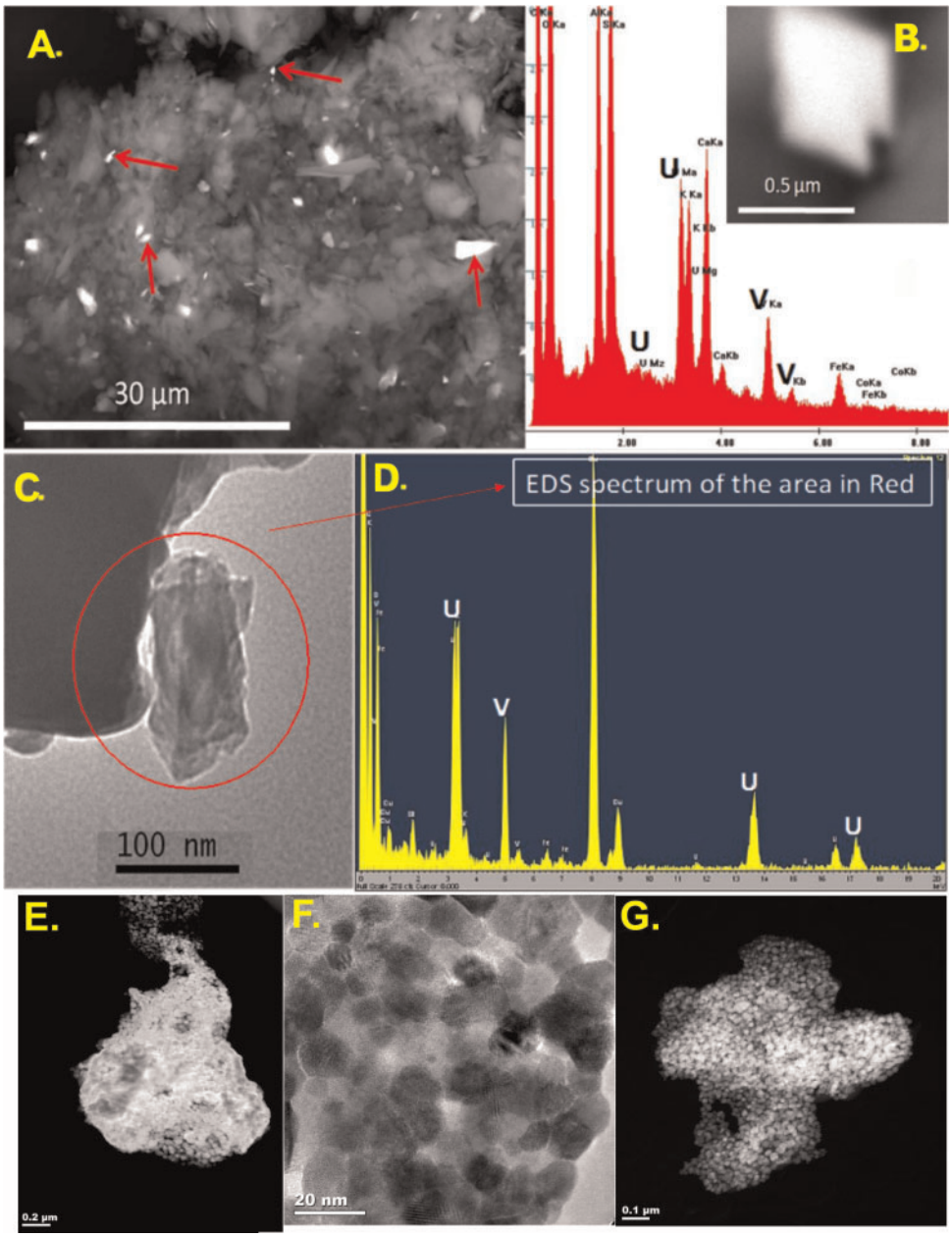

Figure 2. Claim 28 mine site sample contains respirable metallic mineral grains. Transmission electron microscope (TEM) spectroscopic characterizations of sediments (A and B) and submicron grains (arrows) from the Claim 28 mine site reveal respirable-sized grains of carnotite mineral ore, confirmed by spectral analysis (spectrum specific to inset grain in B). Sediments from Claim 28 collected in a cascade impactor following resuspension (C and D) highlight the potential for enrichment of toxic metals in the respirable size fraction. Sediments were resuspended in air and captured in a cascade impactor to characterize respirable fractions. Specifically, respirable particles composed of carnotite, which is a uranyl-vanadate mineral $[K_2(UO_2)_2(VO_4)_2{\cdot}3H_2O]$, can be found in respirable dust from mine sites (C and D). High-resolution TEM imaging of carnotite grains in the Claim 28 PM_{10} samples reveals agglomerated nanocrystals with enhanced surface area (E–G).

significantly different between groups (Figure 5C). Interleukin-6 and KC/GRO levels in the BALF were significantly upregulated following Claim 28 PM_{10} exposure compared with both control ($p < .01$) and Background PM_{10}-treated mice ($p < .05$; Figure 5D). Background PM_{10} treatment did elevate IL-6 and KC/GRO levels significantly above control ($p < .05$). Tumor necrosis factor-alpha, IL-1β, IL-10, IL-2, and IL-5 were also significantly upregulated ($p < .05$) following Claim 28 PM_{10} exposure compared with control; however, background PM_{10} did not cause significant increases in these 5 cytokines relative to control (Figs. 5D and 5E). Interleukin-12p70, IL-4, and IFN-γ were unchanged between treatment groups.

Lung and heart cytokine mRNA expression. Consistent with lavage data, qPCR results indicated that lungs showed significant upregulation of Saa-3 and TNF-α mRNA ($p = .0191$, $p < .0001$) in the Claim 28 PM_{10} group compared with vehicle control (Supplementary Figs. 1A and 1B). Lung IL-1β mRNA was significantly elevated in the Claim 28 PM_{10}-treated group compared with control, while lung IL-1β mRNA in background PM_{10}-treated mice was actually significantly suppressed relative to control (Supplementary Figure 1C). Lung IL-6 mRNA did not significantly vary between treatment groups (Supplementary Figure 1D). The heart appear unaffected by any exposure at 24 h postaspiration, with no significant findings for inflammatory

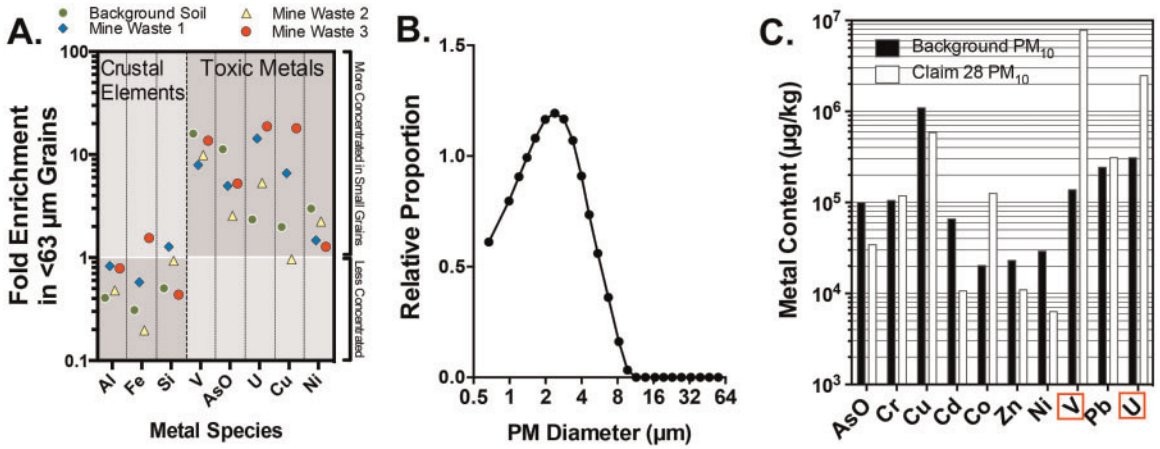

Figure 3. Elemental characterization of sediment and PM_{10} samples. A, Sediment grains < 63 µm (separated by a physical sieve) displayed a relatively greater concentration of numerous toxic metal species, including uranium (U), vanadium (V), and As. Data are shown as the enrichment factor, or ratio of < 63 µm grains compared with the whole sediment sample. Three mine site samples and background sediments are shown. B, Diameters of grains obtained from sediment samples that were resuspended and captured in the next-generation impactor, then resuspended in dispersion media for aspiration treatments were < 10 µm in diameter, as assessed by dynamic light scattering. C, ICP-MS assessment of trace elements in Claim 28 and background PM_{10} samples.

markers Ccl2, Il6, Saa-3, and TNF-α, or for markers of intracellular stress, Nrf2, Hmox1, and NQO1 (Supplementary Figs. 2A–G).

Pulmonary Effects Following Uranyl Acetate and Vanadium Sulfate Oropharyngeal Aspiration

Because U and V were elevated in mine site PM samples compared with background and because these metals are specific to the ore carnotite, we tested whether U and V could independently recapitulate the cardiopulmonary effects of the Claim 28 PM_{10}. Lung lavage contained significantly more total cells following uranyl acetate ($p < .001$) and V sulfate ($p < .0001$) exposure, with V exposure inducing a significantly greater effect than the equimolar dose of U (Figure 6A). Macrophages were significantly upregulated in the V-exposed group alone compared with the vehicle control and U groups ($p < .001$; Figure 6B). Neutrophils were significantly increased in both the U and V exposure groups ($p < .001$) compared with vehicle control, and again V had a greater effect than U (Figure 6C). Total protein was significantly upregulated in the uranyl acetate and V sulfate groups ($p < .001$) relative to control, and V was more potent than U, based on Dunnett's *post hoc* test (Figure 6D).

Bronchoalveolar Lavage Fluid Cytokine Analysis

Several cytokine levels were elevated in the BAL following uranyl acetate and V sulfate aspirations. Interferon-γ and IL-10 were both significantly upregulated in the BAL of mice treated with either PM_{10} sample (Figs. 6E and 6F) and the effect for IL-10 was significantly greater for V than U. Interleukin-5 and IL-6 were both significantly upregulated by V treatment relative to control and U-treated mice, although U exposure alone did induce a modest IL-6 increase (Figs. 6G and 6H).

Several cytokines were more dramatically increased by U compared with the effects of V. This included IL-12p70 and IL-1β, where both metals induced significant effects relative to control but were not statistically different between treatments (Figs. 6I and 6J), as well as KC/GRO and TNF-α, where U effects were significantly and substantially greater than V (Figs. 6K and 6L).

Systemic Effects: Ex Vivo Vasoreactivity and Serum Cytokines

Aortic myography was performed to assess the extrapulmonary effects of the Claim 28 PM_{10} sample. Aortas obtained from mice exposed to Claim 28 PM_{10} exhibited significantly greater vasoreactivity to serotonin than aortas from mice exposed to the background PM_{10} or vehicle control (Figure 7A). As an additional test, we considered the antidilatory impact of serum components, as previously described (Aragon *et al.*, 2015). Naïve aortas (ie, harvested from unexposed WT mice) incubated in the physiological saline bath with 1% serum from both background PM_{10}- or Claim 28 PM_{10}-exposed mice demonstrated significantly reduced ACh-mediated vasorelaxation compared with naïve aortas incubated with serum from vehicle-exposed mice (Figure 7B). An examination of the serum cytokines, using the sample assay panel described for the BAL samples (Figs. 5 and 6), revealed only modest increased in serum concentrations of IL-5 in Claim 28 PM_{10}-exposed mice relative to controls (Figure 7C). All other measured serum cytokines (not shown) were not significantly altered by exposure.

Ex vivo aortic vasoreactivity indicated that both serum obtained from mice after uranyl acetate or V sulfate exposure caused significant impairments in vasorelaxation compared with vehicle control (Figure 8A). Serum IL-5 and IL-6 were profoundly upregulated in V-exposed mice (Figure 8B).

DISCUSSION

Recent findings suggesting that residential proximity to abandoned U mines associated with increased serum inflammatory potential (Harmon *et al.*, 2017) led us to conduct this hazard identification investigation of the pulmonary toxicity of mine site dusts and the principal elemental features of that dust, U, and V. Mine site-derived PM_{10} contained U-V-bearing grains possessing a nanoscale ultrastructure; this observation of seemingly agglomerated, nanometer-sized U-V-bearing particulates was unexpected and is an important consideration for the interpretation of toxic outcomes. Mine waste PM_{10} samples exhibited enhanced cytotoxicity, elicited potentiated pulmonary inflammatory responses, and heightened aortic vasoconstriction to serotonin, compared with a background dust sample derived from

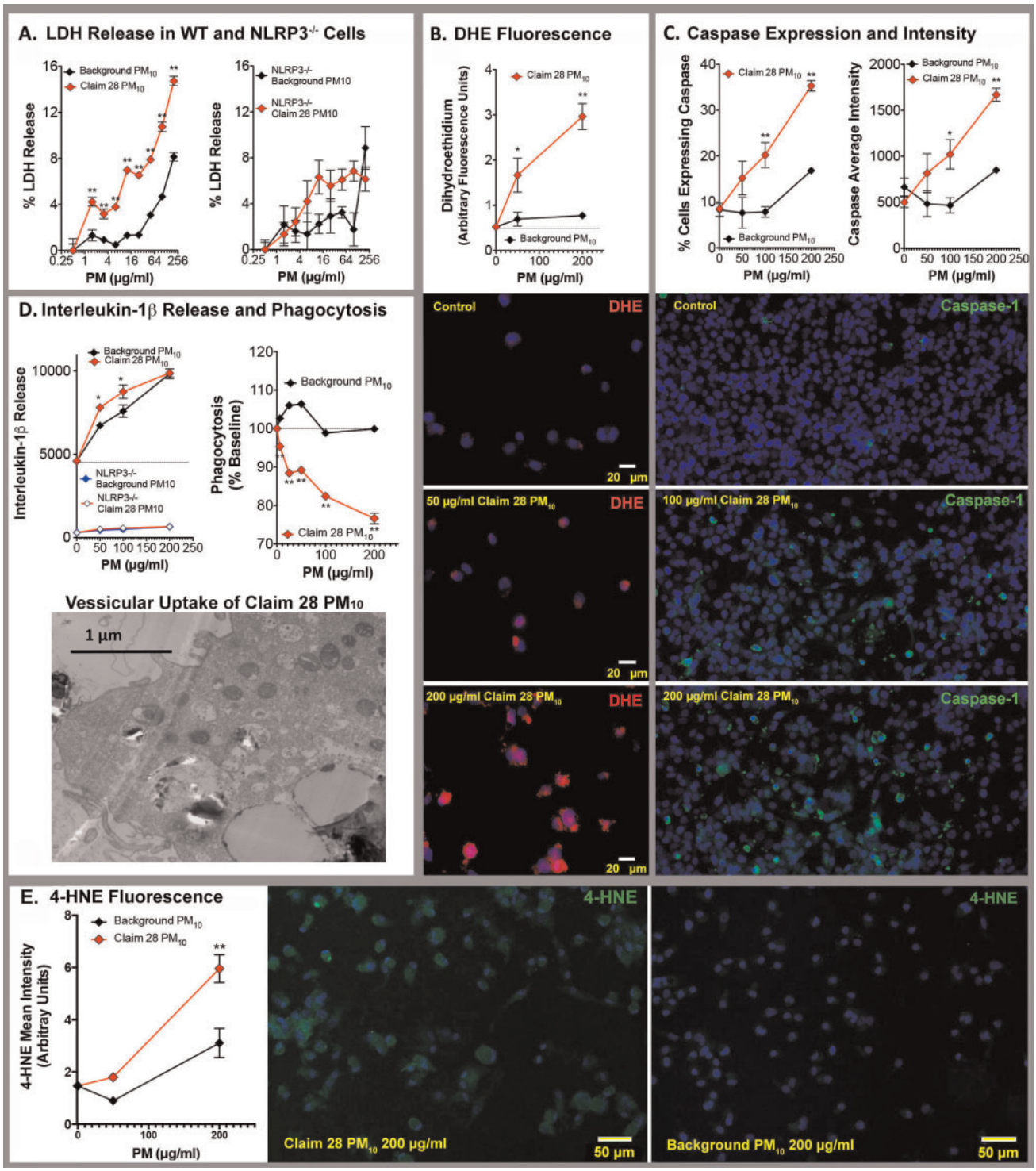

Figure 4. *In vitro* cytotoxicity comparisons of Claim 28 and background PM_{10}. A, Membrane injury in THP-1 cells, as indicated by LDH release was significantly elevated by Claim 28 PM_{10} compared with background PM_{10}, an effect that appeared dependent on NLRP3 ($N = 4$ per group). B, Claim 28 PM_{10}-treated THP-1 cells exhibited greater oxidative stress than background PM_{10}-treated cells, as indicated by dihydroethidium staining (representative images below graph; $N = 3$ per group). C, Caspase-1 expression was similarly increased following Claim 28 PM_{10} compared with background PM_{10} (representative images below graph; $N = 3$ per group). D, Release of IL-1β was slightly elevated, while phagocytic activity was reduced by Claim 28 PM_{10} compared with background PM_{10}($N = 4$ per group). E, 4-Hydroxynonenal staining was elevated in Claim 28 PM_{10} compared with THP-1 cells treated with background PM_{10}. $^{*}p < .05$ and $^{**}p < .01$ compared with background PM_{10} by 2-way ANOVA with a Bonferroni *post hoc* test.

the same region. Furthermore, those metals noted to be in higher concentrations in the mine site dust (U and V) were each able to induce many of these responses, independently. These studies support a possibility that windblown dusts derived from local surface mining operations may incur a greater cardiopulmonary health risk than normal background PM but further

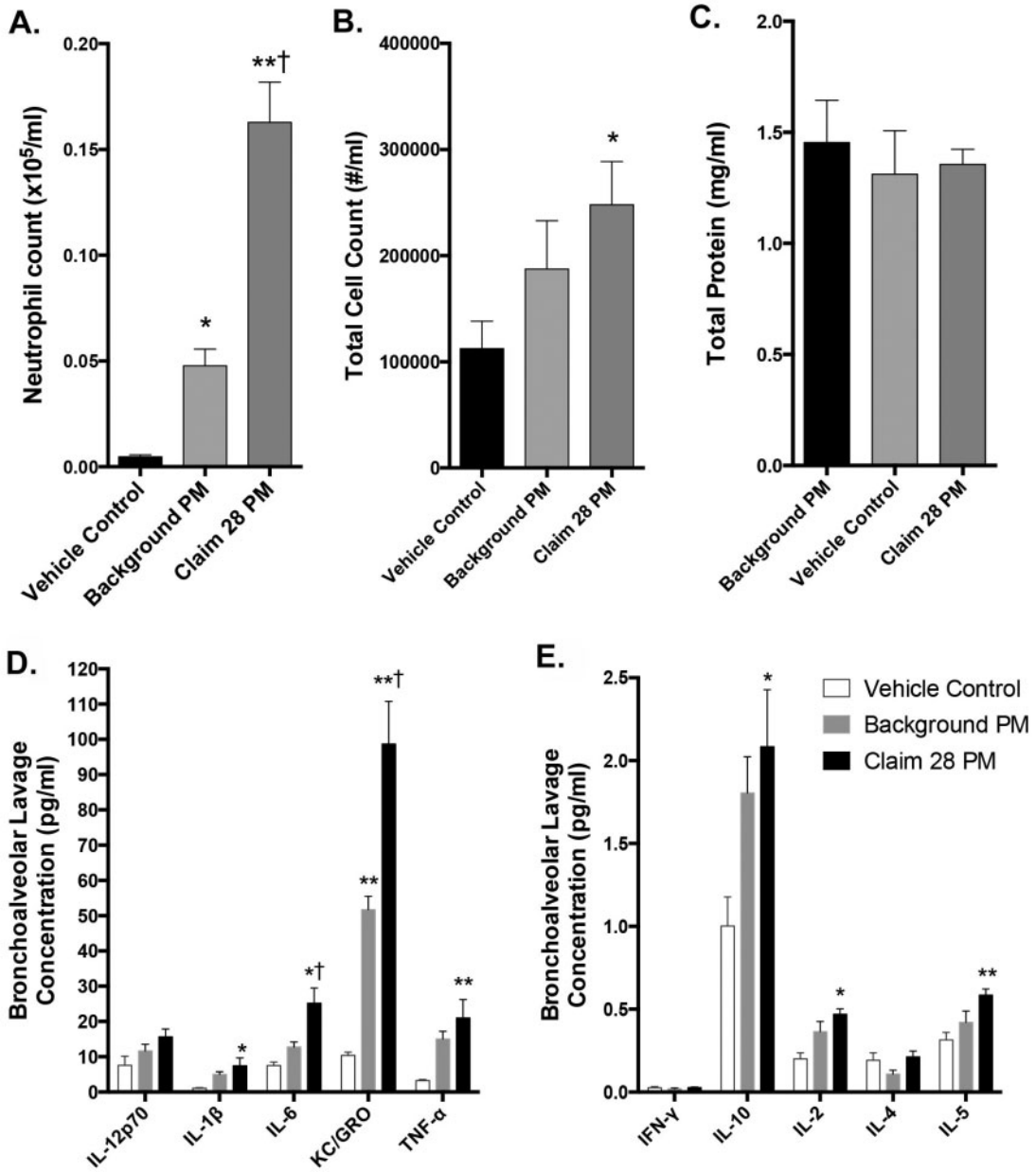

Figure 5. Bronchoalveolar lavage outcomes following oropharyngeal aspirations with Claim 28 and background PM_{10}. Lavage neutrophils (A), total cells (B), and total protein (C) are shown; macrophage counts were not different between groups and not shown. $^{*}p < .05$; $^{**}p < .001$ compared with control; and $\dagger p < .05$ compared with background PM_{10} by 1-way ANOVA with Tukey's *post hoc* test, $N = 6$–8 per group. Lavage cytokines concentrations are also shown. Separate graphs illustrate bronchoalveolar lavage cytokines in greater abundance (D) relative to those in lesser abundance (E) and are thus displayed on different axis scales. $^{*}p < .05$; $^{**}p < .001$ compared with control; and $\dagger p < .05$ compared with background PM_{10} by 1-way ANOVA with Tukey's *post hoc* test, $N = 6$ per group.

research is necessary to fully understand the net exposure dose and health risks in affected communities.

Investigations of Claim 28 mine waste-derived U and other metals suggest that U-V mineral phases similar to carnotite are prevalent in communities located in close proximity to abandoned mines (Blake *et al.*, 2015). Respirable metallic grains isolated in this study appeared to include carnotite ore, based on the relative enrichment with U and V, and these carnotite grains often existed as agglomerated nanoparticles (Figure 2). Nanometer-sized particulates are understood to penetrate deep into the alveolar space (Lanone *et al.*, 2009; Semmler-Behnke *et al.*, 2007), where deposition is greater and retention is prolonged (Geiser and Kreyling, 2010). These particles also possess a greater surface area for reactions with biological materials. Although we were not able to quantify the prevalence of these agglomerated U-V-bearing nanoparticulates, the mine waste PM_{10} was highly cytotoxic compared on an equal mass basis with the background PM but it remains unclear if the morphological and/or chemical differences drive this effect. Furthermore, it remains unclear whether such morphology of the U-containing particulates is a natural phenomenon or a result of mining operations. We posit that repeated wetting and drying of sediments in an oxidative environment may lead to dissolution and recrystallization of these ores near the sediment surface, leading to the formation of nanoscale agglomerates.

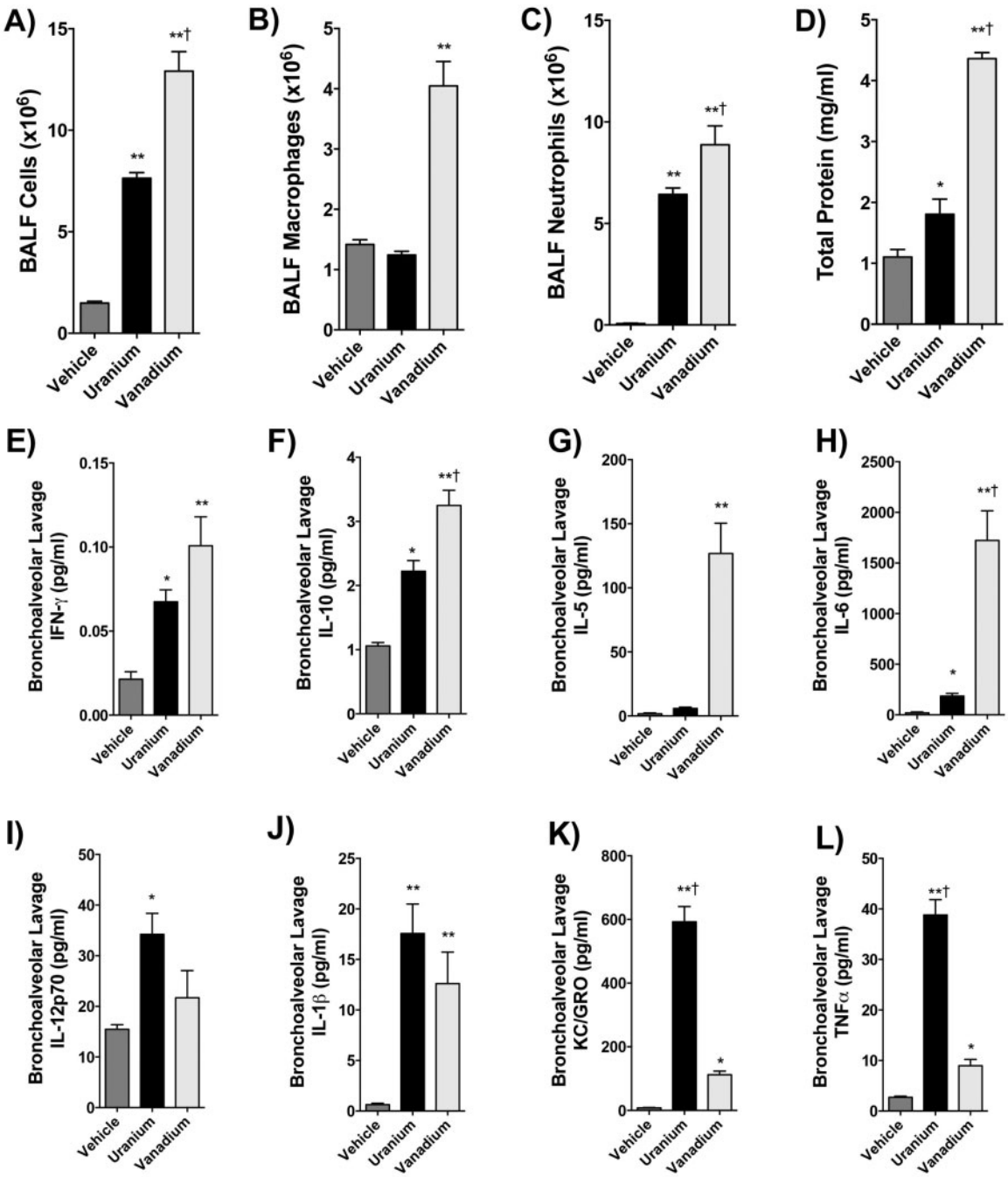

Figure 6. Bronchoalveolar lavage outcomes following oropharyngeal aspirations with 0.22 μmole U or V. Lavage total cells (A), macrophages (B), neutrophils (C), and total protein (D) are shown. $^{*}p < .05$; $^{**}p < .001$ compared with control; and $\dagger p < .05$ compared with background PM by 1-way ANOVA with Tukey's *post hoc* test, $N = 6$ per group. Cytokine analysis of brochoalveolar lavage fluid following U and V pharyngeal aspirations (E–L). Levels of (E) interferon-γ, (F) interleukin (IL)-10, (G) IL-5, and (H) IL-6 were predominantly driven by V, while IL12p70 (I), IL-1β (J), keratinocyte chemoattractant/human growth-regulated oncogene (K), and tumor necrosis factor-alpha (L) were predominantly driven by U. $^{*}p < .05$; $^{**}p < .001$ compared with control; and $\dagger p < .05$ compared with background PM by 1-way ANOVA with Tukey's *post hoc* test, $N = 6$ per group.

Early studies regarding acute toxicity of carnotite ore dust demonstrated that inhalation exposure results in gross lung damage, renal tubular damage and increase in urinary protein following exposure to carnotite (Wilson *et al.*, 1953). Beyond this study, pulmonary and vascular effects following inhaled naturally occurring U and V-containing mineral dusts have not been thoroughly characterized. V, however, has been studied extensively related to its occurrence in ambient PM, especially as a component of residual oil combustion, there is little information regarding the toxicity of U-V-enriched minerals, such as carnotite. High concentrations of V are able to induce pulmonary inflammation and drive adverse cardiovascular outcomes such as bradycardia and arrhythmia in rodents (Campen *et al.*, 2001). Vanadyl sulfate specifically has been noted as a strong Fenton-like generator of free radicals, which may explain its acute toxic potency (Kadiiska *et al.*, 1997). U, on the other hand,

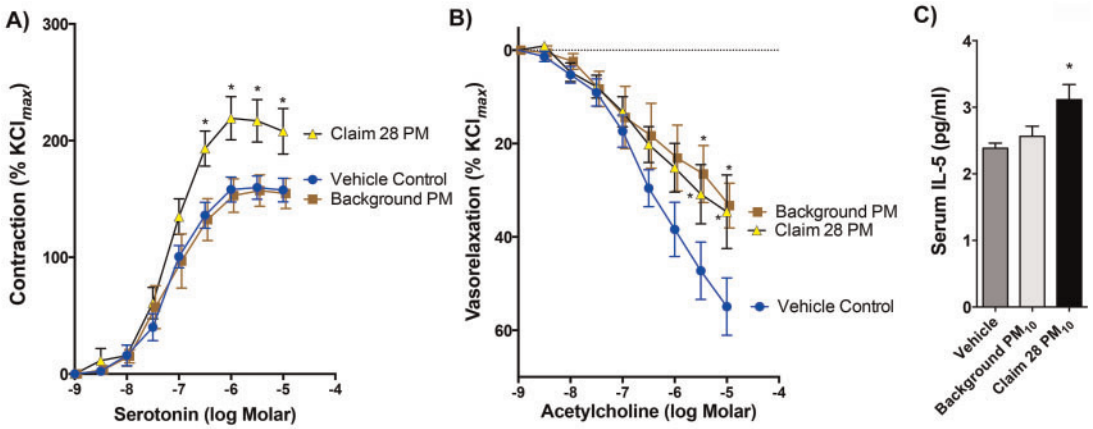

Figure 7. Vasoreactivity and serum cytokine changes following pulmonary exposure to Claim 28 and background PM_{10}. Serotonin-mediated contraction was enhanced following pharyngeal aspirations with Claim 28 PM_{10} compared with vehicle control and Background PM_{10} (A). Asterisks (*) indicate $p < .05$ compared with vehicle control and Background PM_{10} by 2-way ANOVA with Tukey's *post hoc* test, $N = 6$ per group. Serum obtained from both PM_{10}-treated mice, when coincubated with naïve aortic rings (ie, from unexposed mice) significantly impaired acetylcholine-mediated vasorelaxation (B). Of all cytokines measured in the serum (see Materials and Methods), only IL-5 was significantly affected by Claim 28 PM_{10} (C). Asterisk (*) indicates significant difference from control ($p < .05$) by ANOVA with Tukey's *post hoc* test, $N = 6$ per group.

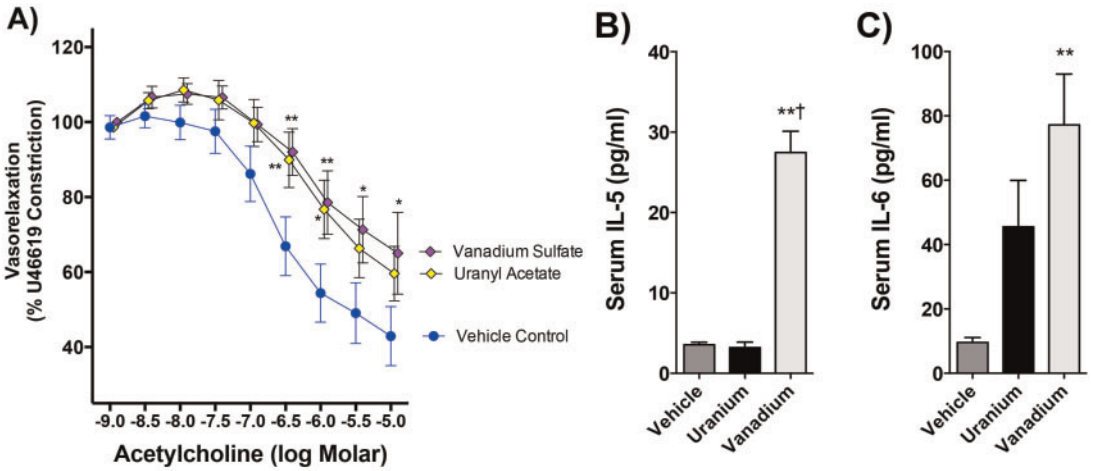

Figure 8. Vasoreactivity and serum cytokine effects of pulmonary uranium and vanadium exposure. Acetylcholine-mediated relaxation was impaired following pharyngeal aspirations with 0.22 μmols U and V in 50 μl vehicle (A). Values are statistically significant at $p < .05$. *$p < .05$ and **$p < .001$ by 2-way ANOVA, $N = 6$ per group. Only pulmonary exposure to V induced both IL-5 (B) and IL-6 (C) levels in the circulation. No other cytokines measured in serum (see Materials and Methods) showed any significant change compared with control. **$p < .001$ compared with control and †$p < .01$ compared with uranium by 1-way ANOVA with Tukey's *post hoc* test, $N = 6$ per group.

has not been extensively studied as an inhaled toxin. In this study, uranyl acetate and $VOSO_4$ each produced inflammatory responses in the lung, although with somewhat dichotomous trends in the pattern of cytokines released. Uranyl acetate produced a classic innate immune response with increased pulmonary neutrophilia and elevated KC/GRO, IL-1β, and TNF-α. Pulmonary exposure to $VOSO_4$, on the other hand, led to significant recruitment of macrophages to the airway and produced a cytokine pattern more consistent with a T_H2-like response with elevated IL-5 and IL-6. Further research on the intracellular oxidation of U-V-containing PM within macrophages is needed to confirm whether uranyl-vanadate minerals actually dissociate *in vivo*, and if so, whether those isolated metal ions drive the observed toxicity.

In vitro assays revealed outcomes that were perhaps more profound than the *in vivo* effects. The dramatic cytotoxicity and cellular injury differences between Claim 28 and background PM_{10} at high concentrations (50–200 μg/ml) were driven by NLRP3-dependent inflammasomal pathways. Interestingly, cytotoxicity was observed at the lowest tested concentrations (1.5 μg/ml) for Claim 28 PM_{10} that appeared NLRP3 independent, suggesting additional mechanisms of toxicity not observed for background PM_{10}. THP-1 cells were able to engulf particulates from both samples but phagocytic activity to a secondary challenge was reduced even at the lowest concentration of Claim 28 PM_{10} compared with background PM_{10}. Although IL-1β release in THP-1 cells was only modestly different, we did observe profound differences in IL-1β mRNA expression (whole lung) and protein level (lavage) in Claim 28 PM_{10}-treated lungs. More detailed cellular mechanistic work is needed to understand the impacts that carnotite-bearing PM may specifically have on phagocytic cells, as this could negatively impact host defense and immunological responses.

The physicochemical differences between these PM_{10} samples are numerous and this study only examined the possibility that U and/or V as soluble ions were principal drivers of toxicity.

Parameters like surface area, reactivity, and composition all have the potential to contribute to the cellular and *in vivo* responses. Previous studies have utilized the approach of studying the soluble metal components to confirm a role for PM chemistry as a modifier of toxicity. Residual oil fly ash was notable for the presence of several highly soluble metals, including V, iron, and nickel, which could directly and independently drive pulmonary inflammation, hypothermia, and bradycardia/bradyarrhythmias (Campen *et al.*, 2002; Costa and Dreher, 1997; Dreher *et al.*, 1997; Kodavanti *et al.*, 1998). Furthermore, interactive toxicity was noted for the combination of V and nickel (Campen *et al.*, 2001). $VOSO_4$ was specifically noted as a driver of Fenton-like radical generation, which is thought to be central to its pulmonary toxicity (Kadiiska *et al.*, 1997). There are, however, considerable uncertainties in the use of soluble metal salts to reproduce the effects of particulate-bound metals. For one, we are uncertain of the chemical dissolution forms of U and V arising from carnotite ore, which is complicated even further by the anatomical location where dissolution occurs. Certainly, a phagolysosome will generate a complex mixture of solvents, including hydrogen peroxide and hypochlorite, in a reduced pH environment in an attempt to digest particulates; the influence of this intracellular process on carnotite (or other U ores) solubility is unknown. Additionally, the particulate form itself may mechanically interact with cellular scavenger receptors and other molecules to induce inflammatory responses and cytoskeletal rearrangements that would not be activated by soluble metals (Obot *et al.*, 2002; Thakur *et al.*, 2009; Wang *et al.*, 2017). Studies with manual metal arc stainless steel welding fumes indicated that pulmonary inflammation and injury was dependent on both the soluble and insoluble metals (Taylor *et al.*, 2003), while other *in vitro* studies with nickel-based welding fumes noted that soluble fractions drove most toxicity and could be abrogated with metal chelators (McNeilly *et al.*, 2004). Thus, while the U and V results offer mechanistic clues as to how mine site-derived PM may exhibit enhanced toxicity, this is only a preliminary approach and more complex studies are needed to fully understand the *in vivo* mechanisms of pulmonary toxicity.

An important caveat to these studies is the high dose approach used, which, while not directly relevant to human environmental exposures, was vital to directly comparing the potency of respirable dusts from mine waste and background sediment samples. The clear pulmonary toxicity of mine site dusts was inherent to the hazard identification study design and must be put into the context of relevant environmental exposures. Currently, the magnitude of community exposure remains uncertain but the duration of residence is known to be longer than 30 years (Harmon *et al.*, 2016, 2017). Efforts to model airborne exposures suggest that prevailing winds are sufficient to move contaminants but at low levels (Stovern *et al.*, 2014). Aeolian resuspension in arid climates occur at fairly common wind speeds ranging from 6 to 10 m/s (13–20 mph), depending on the characteristics of sediment (Jugder *et al.*, 2014). Similar studies have noted that PM_{10} arising during windstorms in mining regions leads to greater heavy metal contamination and more potent PM toxicity (Xiao *et al.*, 2014). Furthermore, the size of the mine site relative to the surrounding affected territory is an additional factor in considering potential community exposures. Importantly, animal toxicology studies have certain value for identifying inhalational hazards and comparing PM toxicity but environmental protection policies have emphasized epidemiological relationships with ambient PM concentrations, due to the relative insensitivity of rodents to PM-associated health effects. Active air monitoring of the region with a relatively specific chemical tracer such as U should be an effective approach for exposure assessment, facilitating a more refined examination of mine-derived PM-associated health effects in the Navajo communities.

CONCLUSIONS

Abandoned or partially remediated surface U mine sites exist throughout the Navajo Nation and Rocky Mountain region of the United States and it is estimated that over 280 000 Native Americans live within 10 km of a U mine site (Lewis *et al.*, 2017). Observations of enhanced *in vitro* and *in vivo* toxicity of PM_{10} containing residual U-V-bearing minerals with a nanoparticulate ultrastructure in sediments vulnerable to Aeolian transport raise concerns for windblown transport and community or occupational inhalational exposures, and bring into question the long-term effectiveness of past remediation efforts. Although the overall contribution to ambient PM is expected to be exceedingly low, local residents within a few kilometers of mine sites may have lived in their residence for many decades. A more thorough assessment of inhalational exposure is therefore warranted to better understand the potential health risks from this site and similar abandoned mines throughout the country.

SUPPLEMENTARY DATA

Supplementary data are available at *Toxicological Sciences* online.

ACKNOWLEDGMENTS

The authors sincerely thank Blue Gap Tachee, AZ community members Sadie Bill, Aaron Yazzie, and Christopher Nez, and the Navajo Nation for their continuing support of these studies. They also thank Sherri Friend and Diane Schwegler-Berry for their assistance with electron microscopy.

FUNDING

National Institute of Environmental Health Sciences (R01 ES026673, P42 ES025589); Academic Science Education and Research Training (ASERT) program (K12GM088021 to K.E.Z.). The findings and conclusions in this report are those of the authors and do not necessarily represent the views of the National Institute for Occupational Safety and Health.

AUTHOR CONTRIBUTIONS

K.E.Z. helped design the overall study and executed or provided oversight to most facets, including sample preparation, exposure, and data analysis. V.K. conducted *in vitro* studies, analyzed data, and helped write the article. M.H., C.R.T., B.S., and A.W. all contributed to executing the exposures, analyzing data, and editing the article. G.H. supported the exposures and collection/analysis of pulmonary inflammation data. S.A. and J.M.C. helped to prepare samples for exposure and conducted the chemical analysis and TEM imaging, as well as helped to write the article. N.K.K. and P.M. performed NGI collections of particulate fraction and characterized the distribution in the DM, as well as helped write and edit the article. C.S. identified the concerns of the Blue Gap Tachee Native American community, bringing this

issue to the inhalation toxicology laboratory at UNM, provided collections of initial samples for research, and helped write the article. A.B. provided HR-TEM and XANES analysis of material and helped write the article. A.-M.A. Supported the analytical chemistry for ICP-MS and ICP-OES characterization of particulates and sediments and helped edit the article. Y.L. provided geospatial expertise to help locate samples of interest and provide illustrative descriptions of the locale, as well as provide edits for the article. M.S. supported the execution and analysis of *in vitro* studies, conducted zeta, and sizing characterizations of PM for *in vitro* studies and helped edit the article. A.E. consulted on the overall project, especially the design of *in vitro* toxicology assessments, provided funding, and helped write and edit the article. M.J.C. helped conceive the project and study design, obtained funding, analyzed data, and wrote/edited the article.

REFERENCES

Aragon, M., Erdely, A., Bishop, L., Salmen, R., Weaver, J., Liu, J., Hall, P., Eye, T., Kodali, V., Zeidler-Erdely, P., *et al.* (2016). MMP-9-dependent serum-borne bioactivity caused by multiwalled carbon nanotube exposure induces vascular dysfunction via the CD36 scavenger receptor. *Toxicol. Sci.* **150**, 488–498.

Aragon, M. J., Chrobak, I., Brower, J., Roldan, L., Fredenburgh, L. E., McDonald, J. D., and Campen, M. J. (2015). Inflammatory and vasoactive effects of serum following inhalation of varied complex mixtures. *Cardiovasc. Toxicol.* **2**, 1–9.

Arfsten, D. P., Still, K. R., and Ritchie, G. D. (2001). A review of the effects of uranium and depleted uranium exposure on reproduction and fetal development. *Toxicol. Ind. Health* **17**, 180–191.

Bell, M. L., Ebisu, K., Peng, R. D., Samet, J. M., and Dominici, F. (2009). Hospital admissions and chemical composition of fine particle air pollution. *Am. J. Respir. Crit. Care Med.* **179**, 1115–1120.

Blake, J. M., Avasarala, S., Artyushkova, K., Ali, A.-M. S., Brearley, A. J., Shuey, C., Robinson, W. P., Nez, C., Bill, S., Lewis, J., *et al.* (2015). Elevated concentrations of U and co-occurring metals in abandoned mine wastes in a northeastern Arizona Native American community. *Environ. Sci. Technol.* **49**, 8506–8514.

Bradford, M. M. (1976). A rapid and sensitive method for the quantitation of microgram quantities of protein utilizing the principle of protein-dye binding. *Anal. Biochem.* **72**, 248–254.

Brook, R. D., Rajagopalan, S., Pope, C. A., III, Brook, J. R., Bhatnagar, A., Diez-Roux, A. V., Holguin, F., Hong, Y., Luepker, R. V., Mittleman, M. A., *et al.* (2010). Particulate matter air pollution and cardiovascular disease: An update to the scientific statement from the American Heart Association. *Circulation* **121**, 2331–2378.

Brugge, D., Benally, T., and Yazzie-Lewis, E. (2007). *The Navajo People and Uranium Mining*. UNM Press, Albuquerque, NM.

Brugge, D., deLemos, J. L., and Oldmixon, B. (2005). Exposure pathways and health effects associated with chemical and radiological toxicity of natural uranium: A review. *Rev. Environ. Health* **20**, 177–194.

Campen, M. J., Nolan, J. P., Schladweiler, M. C., Kodavanti, U. P., Costa, D. L., and Watkinson, W. P. (2002). Cardiac and thermoregulatory effects of instilled particulate matter-associated transition metals in healthy and cardiopulmonary-compromised rats. *J. Toxicol. Environ. Health A* **65**, 1615–1631.

Campen, M. J., Nolan, J. P., Schladweiler, M. C. J., Kodavanti, U. P., Evansky, P. A., Costa, D. L., and Watkinson, W. P. (2001). Cardiovascular and thermoregulatory effects of inhaled PM-associated transition metals: A potential interaction between nickel and vanadium sulfate. *Toxicol. Sci.* **64**, 243–252.

Costa, D. L., and Dreher, K. L. (1997). Bioavailable transition metals in particulate matter mediate cardiopulmonary injury in healthy and compromised animal models. *Environ. Health Perspect.* **105**, 1053–1060.

Dawson, S. E., Charley, P. H., and Harrison, P. (1997). Advocacy and social action among Navajo uranium workers and their families. In *Social Work in Health Settings: Practice in Context*, pp. 391–407.

deLemos, J. L., Brugge, D., Cajero, M., Downs, M., Durant, J. L., George, C. M., Henio-Adeky, S., Nez, T., Manning, T., Rock, T., *et al.* (2009). Development of risk maps to minimize uranium exposures in the Navajo Churchrock mining district. *Environ. Health* **8**, 29.

Dominici, F., Peng, R. D., Ebisu, K., Zeger, S. L., Samet, J. M., and Bell, M. L. (2007). Does the effect of PM10 on mortality depend on PM nickel and vanadium content? A reanalysis of the NMMAPS data. *Environ. Health Perspect.* **115**, 1701–1703.

Dreher, K. L., Jaskot, R. H., Lehmann, J. R., Richards, J. H., McGee, J. K., Ghio, A. J., and Costa, D. L. (1997). Soluble transition metals mediate residual oil fly ash induced acute lung injury. *J. Toxicol. Environ. Health* **50**, 285–305.

Geiser, M., and Kreyling, W. G. (2010). Deposition and biokinetics of inhaled nanoparticles. *Part. Fibre Toxicol.* **7**, 2.

Gittelsohn, J., Kim, E. M., He, S., and Pardilla, M. (2013). A food store-based environmental intervention is associated with reduced BMI and improved psychosocial factors and food-related behaviors on the Navajo nation. *J. Nutr.* **143**, 1494–1500.

Harmon, M. E., Campen, M. J., Miller, C., Shuey, C., Cajero, M., Lucas, S., Pacheco, B., Erdei, E., Ramone, S., Nez, T., *et al.* (2016). Associations of circulating oxidized LDL and conventional biomarkers of cardiovascular disease in a cross-sectional study of the Navajo population. *PLoS One* **11**, e0143102.

Harmon, M. E., Lewis, J., Miller, C., Hoover, J., Ali, A. S., Shuey, C., Cajero, M., Lucas, S., Zychowski, K., Pacheco, B., *et al.* (2017). Residential proximity to abandoned uranium mines and serum inflammatory potential in chronically exposed Navajo communities. *J. Expo. Sci. Environ. Epidemiol.* **27**, 365–371.

Homma-Takeda, S., Kitahara, K., Suzuki, K., Blyth, B. J., Suya, N., Konishi, T., Terada, Y., and Shimada, Y. (2015). Cellular localization of uranium in the renal proximal tubules during acute renal uranium toxicity. *J. Appl. Toxicol.* **35**, 1594–1600.

Hoover, J., Gonzales, M., Shuey, C., Barney, Y., and Lewis, J. (2017). Elevated arsenic and uranium concentrations in unregulated water sources on the Navajo Nation, USA. *Expo. Health* **9**, 113–124.

Jugder, D., Shinoda, M., Kimura, R., Batbold, A., and Amarjargal, D. (2014). Quantitative analysis on windblown dust concentrations of PM10 (PM2.5) during dust events in Mongolia. *Aeolian Res.* **14**, 3–13.

Kadiiska, M. B., Mason, R. P., Dreher, K. L., Costa, D. L., and Ghio, A. J. (1997). In vivo evidence of free radical formation in the rat lung after exposure to an emission source air pollution particle. *Chem. Res. Toxicol.* **10**, 1104–1108.

Kodavanti, U. P., Hauser, R., Christiani, D. C., Meng, Z. H., McGee, J., Ledbetter, A., Richards, J., and Costa, D. L. (1998). Pulmonary responses to oil fly ash particles in the rat differ

by virtue of their specific soluble metals. *Toxicol. Sci.* **43**, 204–212.

Lanone, S., Rogerieux, F., Geys, J., Dupont, A., Maillot-Marechal, E., Boczkowski, J., Lacroix, G., and Hoet, P. (2009). Comparative toxicity of 24 manufactured nanoparticles in human alveolar epithelial and macrophage cell lines. *Part. Fibre Toxicol.* **6**, 14.

Lewis, J., Hoover, J., and MacKenzie, D. (2017). Mining and environmental health disparities in native American communities. *Curr. Environ. Health Rep.* **4**, 130–141.

Lippmann, M., Ito, K., Hwang, J. S., Maciejczyk, P., and Chen, L. C. (2006). Cardiovascular effects of nickel in ambient air. *Environ. Health Perspect.* **114**, 1662–1669.

Livak, K. J., and Schmittgen, T. D. (2001). Analysis of relative gene expression data using real-time quantitative PCR and the $2^{-\Delta\Delta CT}$ method. *Methods* **25**, 402–408.

McNeilly, J. D., Heal, M. R., Beverland, I. J., Howe, A., Gibson, M. D., Hibbs, L. R., MacNee, W., and Donaldson, K. (2004). Soluble transition metals cause the pro-inflammatory effects of welding fumes in vitro. *Toxicol. Appl. Pharmacol.* **196**, 95–107.

Mulloy, K. B., James, D. S., Mohs, K., and Kornfeld, M. (2001). Lung cancer in a nonsmoking underground uranium miner. *Environ. Health Perspect.* **109**, 305.

Munson, S. M., Belnap, J., and Okin, G. S. (2011). Responses of wind erosion to climate-induced vegetation changes on the Colorado Plateau. *Proc. Natl. Acad. Sci.* **108**, 3854–3859.

Nadadur, S. S., Haykal-Coates, N., Mudipalli, A., and Costa, D. L. (2009). Endothelial effects of emission source particles: Acute toxic response gene expression profiles. *Toxicol. In Vitro* **23**, 67–77.

Ngwa, H. A., Kanthasamy, A., Jin, H., Anantharam, V., and Kanthasamy, A. G. (2014). Vanadium exposure induces olfactory dysfunction in an animal model of metal neurotoxicity. *Neurotoxicology* **43**, 73–81.

Obot, C. J., Morandi, M. T., Beebe, T. P., Hamilton, R. F., and Holian, A. (2002). Surface components of airborne particulate matter induce macrophage apoptosis through scavenger receptors. *Toxicol. Appl. Pharmacol.* **184**, 98–106.

Paffett, M. L., Zychowski, K. E., Sheppard, L., Robertson, S., Weaver, J. M., Lucas, S. N., and Campen, M. J. (2015). Ozone inhalation impairs coronary artery dilation via intracellular oxidative stress: Evidence for serum-borne factors as drivers of systemic toxicity. *Toxicol. Sci.* **146**, 244–253.

Percy, C., Freedman, D. S., Gilbert, T. J., White, L., Ballew, C., and Mokdad, A. (1997). Prevalence of hypertension among Navajo Indians: Findings from the Navajo Health and Nutrition Survey. *J. Nutr.* **127**, 2114S–2119S.

Peters, A., and Pope, C. A., III. (2002). Cardiopulmonary mortality and air pollution. *Lancet* **360**, 1184–1185.

Poisson, C., Stefani, J., Manens, L., Delissen, O., Suhard, D., Tessier, C., Dublineau, I., and Guéguen, Y. (2014). Chronic uranium exposure dose-dependently induces glutathione in rats without any nephrotoxicity. *Free Radic. Res.* **48**, 1218–1231.

Pope, C. A., III, Burnett, R. T., Thurston, G. D., Thun, M. J., Calle, E. E., Krewski, D., and Godleski, J. J. (2003). Cardiovascular mortality and long-term exposure to particulate air pollution: Epidemiological evidence of general pathophysiological pathways of disease. *Circulation* **109**, 71–77.

Robertson, S., Colombo, E. S., Lucas, S. N., Hall, P. R., Febbraio, M., Paffett, M. L., and Campen, M. J. (2013). CD36 mediates endothelial dysfunction downstream of circulating factors induced by O3 exposure. *Toxicol. Sci.* **134**, 304–311.

Saint-Marc, B., Elie, C., Manens, L., Tack, K., Benderitter, M., Gueguen, Y., and Ibanez, C. (2016). Chronic uranium contamination alters spinal motor neuron integrity via modulation of SMN1 expression and microglia recruitment. *Toxicol. Lett.* **254**, 37–44.

Semmler-Behnke, M., Takenaka, S., Fertsch, S., Wenk, A., Seitz, J., Mayer, P., Oberdörster, G., and Kreyling, W. G. (2007). Efficient elimination of inhaled nanoparticles from the alveolar region: Evidence for interstitial uptake and subsequent reentrainment onto airways epithelium. *Environ. Health Perspect.* **115**, 728–733.

Stokes, W. L. (1951). *Carnotite Deposits in the Carrizo Mountains Area, Navajo Indian Reservation, Apache County, Arizona and San Juan County, New Mexico*. USGS Circular 111.

Stovern, M., Felix, O., Csavina, J., Rine, K. P., Russell, M. R., Jones, R. M., King, M., Betterton, E. A., and Sáez, A. E. (2014). Simulation of windblown dust transport from a mine tailings impoundment using a computational fluid dynamics model. *Aeolian Res.* **14**, 75–83.

Taylor, M. D., Roberts, J. R., Leonard, S. S., Shi, X., and Antonini, J. M. (2003). Effects of welding fumes of differing composition and solubility on free radical production and acute lung injury and inflammation in rats. *Toxicol. Sci.* **75**, 181–191.

Thakur, S. A., Hamilton, R., Jr, Pikkarainen, T., and Holian, A. (2009). Differential binding of inorganic particles to MARCO. *Toxicol. Sci.* **107**, 238–246.

Vicente-Vicente, L., Quiros, Y., Perez-Barriocanal, F., Lopez-Novoa, J. M., Lopez-Hernandez, F. J., and Morales, A. I. (2010). Nephrotoxicity of uranium: Pathophysiological, diagnostic and therapeutic perspectives. *Toxicol. Sci.* **118**, 324–347.

Wang, T., Shimizu, Y., Wu, X., Kelly, G. T., Xu, X., Wang, L., Qian, Z., Chen, Y., and Garcia, J. G. N. (2017). Particulate matter disrupts human lung endothelial cell barrier integrity via Rho-dependent pathways. *Pulm. Circ.* **7**, 617–623.

Wilson, H. B., Stokinger, H. E., and Sylvester, G. E. (1953). Acute toxicity of carnotite ore dust. *Arch. Ind. Hyg. Occup. Med.* **7**, 301–309.

Xia, T., Hamilton, R. F., Bonner, J. C., Crandall, E. D., Elder, A., Fazlollahi, F., Girtsman, T. A., Kim, K., Mitra, S., Ntim, S. A., *et al.* (2013). Interlaboratory evaluation of in vitro cytotoxicity and inflammatory responses to engineered nanomaterials: The NIEHS Nano GO Consortium. *Environ. Health Perspect.* **121**, 683–690.

Xiao, Z. H., Shao, L. Y., Zhang, N., Wang, J., Chuang, H. C., Deng, Z. Z., Wang, Z., and BeruBe, K. (2014). A toxicological study of inhalable particulates in an industrial region of Lanzhou City, northwestern China: Results from plasmid scission assay. *Aeolian Res.* **14**, 25–34.